# Phase Separation and Dewetting of Weakly Incompatible Polymer Blend Films

**P. Müller-Buschbaum,*,† S. A. O'Neill,‡ S. Affrossman,‡ and M. Stamm†**

*Max-Planck-Institut für Polymerforschung, Ackermannweg 10, 55021 Mainz, Germany, Department of Pure and Applied Chemistry, University of Strathclyde, Cathedral Street, Glasgow G1 1XL, U.K.*

*Received December 10, 1997; Revised Manuscript Received April 2, 1998*

ABSTRACT: The phase separation and dewetting of thin films of blends of deuterated polystyrene (dPS) and poly(*p*-methylstyrene) (PpMS) were investigated during annealing. The surface morphology, obtained from atomic force microscopy and phase measurement interference microscopy, the density profile, determined by X-ray reflectivity in the region of total external reflection, and the surface composition obtained from static secondary ion mass spectroscopy, are reported. This system is only weakly incompatible. The interaction of the components with substrate and air during phase separation leads to a bilayer formation with a broad polymer−polymer interface. PpMS segregates to the air interface. The bilayer structure is unstable and defines the starting point for the dewetting of PpMS on top of the dPS layer. In the final dewetting state a homogeneous layer of dPS on top of the substrate is covered with an ultrathin layer of PpMS as well as with quite thick mesoscopic drops of PpMS.

## Introduction

Thin polymer blend films are of special interest for technological applications as well as for fundamental investigations. The technological interest is focused on the specific properties of the polymer blends and thus on controlling morphology and phase composition. This has motivated many fundamental studies about the phase separation of polymer blends.[1] The dewetting of phase separated blends displays the limitations of any high-tech application, which requires a stable, homogeneous and uniform film. While most dewetting studies have dealt with thin liquid films on top of solid substrates (e.g., refs 2−5) the dewetting at the liquid−liquid interface of thick[6] or thin films[7,8] was only recently studied. Avoiding all difficulties related with the sample preparation via flotation, we present a bilayer formation via phase separation of a weakly incompatible polymer blend. *In bulk systems*, unlike the more familiar nucleation and growth mechanism, a phase separation caused by spinodal decomposition is observed. The free energy is decreased by small amplitude composition fluctuations that grow exponentially with time as a result of up-gradient diffusion. The magnitude of the randomly oriented wave vector of the composition wave is close to the fastest growing wave of wave vector $q_m$. At longer times, however, the phase-separating structure coarsens and the magnitude of $q_m$ decreases. *In thin films of polymer blends* the situation is qualitatively different[9] because the blend is confined between two different interfaces (one toward the substrate and one toward the air). Depending on the nature of long- and short-range interactions[10] between the polymers and the interfaces, an affinity for one of the components results. When the polymer blend is quenched into the unstable two-phase region, this leads to a strongly varying composition profile perpendicular to the substrate surface. This surface-directed spinodal decomposition is suppressed for films of thicknesses thinner than the characteristic spinodal wavelength,[11−13] which is on the order of 1000 Å, as measurements of Krausch et al.[14] suggest. Therefore, a dimensional crossover in the phase separation kinetics is observable in thin polymer blend films.[15]

Choosing a binary mixture of polymer A and polymer B for which one component has an affinity for the substrate interface and one for the air interface favors a phase separation into two layers. Focusing on the interface between both polymers, this sample preparation via phase separation defines a better starting condition for a dewetting experiment compared to a bilayer system built with the floating technique (one of the films is floated off onto distilled water and picked up by the other film, which is still on the substrate): Despite a small amount of polymer A solved in the phase of polymer B and vice versa, the width of the interface between polymer A and B is controlled by the compatibility of both,[16] whereas in systems built up by the floating-technique small cavities, some amount of water and folds at the interface cannot be avoided. Nevertheless, the variety of binary polymer mixtures is limited because blends that exhibit a marked surface morphology induced by phase separation during the spin-coating of the blend[17−20] are not suited.

Therefore, we chose as a model system deuterated polystyrene (dPS) and poly(*p*-methylstyrene) (PpMS), which is a weakly incompatible blend.[21−23] The free film boundary was examined with optical phase measurement interference microscopy (PMIM), with atomic-force microscopy (AFM), and with static secondary ion mass spectroscopy (static SIMS). The density profile perpendicular to the substrate surface was measured with X-ray reflectivity in the region of total external reflection. With annealing times up to 911 h, the phase separation building the bilayer system and the dewetting of the upper PpMS layer on top of the dPS layer were followed. Our data indicate that the dewetting process is due to spinodal decomposition.

The introduction is followed by an Experimental Section describing the sample preparation and the techniques used. The next section deals with the interpretation of the X-ray measurements. Then the

† Max-Planck-Institut für Polymerforschung.
‡ University of Strathclyde.

S0024-9297(97)01802-0 CCC: $15.00 
Published on Web 06/27/1998

AFM, PMIM, and static SIMS measurements are reported. A discussion and summary conclude the paper.

## Experimental Section

**Sample Preparation.** Deuterated polystyrene (dPS) with a molecular weight $M_w = 157\,000$ and a narrow molecular weight distribution $M_w/M_N = 1.09$ as well as poly(*p*-methylstyrene) (PpMS) with a molecular weight $M_w = 161\,000$ g/mol and $M_w/M_N = 1.05$ are used. Samples (25 mg) of each were dissolved in 5 mL of toluene; consequently, for this investigation the dPS/PpMS blend films have a symmetric composition (50% weight fraction of each). The thin film blend samples were cast on silicon substrates by spin-coating (4000 rpm for 30s) from a toluene solution of the blend. Prior to spin-coating, the silicon substrates were cleaned in a bath of 100 mL of 80% $H_2SO_4$, 35 mL of $H_2O_2$, and 15 mL of deionized water for 15 min at 80 °C and rinsed in deionized water. The silicon surface was dried with compressed nitrogen. From X-ray reflectivity measurements right after preparation, the film thickness of the blend films presented was determined to be $l = 504 \pm 9$ Å. To check the reproducibility of observed structures over a larger film thickness range, additional samples from 360 to 510 Å were prepared and examined. The as-cast samples as well as the annealed samples exhibit the same morphologies as described below. In the dewetting structure the size of the drops is decreased with decreasing film thickness of the once homogeneous film, keeping the morphological features. Only the time scale is affected if the film thickness is different in the way that thinner films show an earlier phase separation and dewetting compared to thicker ones. Additionally, samples cut into smaller pieces show an accelerated dewetting due to introduced defects without changing the appearing morphologies. Therefore, special care in the film preparation and treatment has to be taken to get the time scale.

The samples were examined as prepared and then annealed for several periods to create the bilayer configuration and to observe dewetting. The annealing temperature $T = 154$ °C corresponds to a temperature well within the two-phase regime of the dPS/PpMS phase diagram.

**X-ray Reflectivity.** The X-ray experiments in the region of total external reflection were performed with a reflectometer with a 18 kW rotating anode and a copper target. With a graphite monochromator and a slit collimating system, a beam divergence of 0.01° and a wavelength $\lambda = 1.54$ Å were chosen. The in-plane coherence length, which gives the size of the coherently illuminated surface area, is estimated with 100 $\mu$m for small incidence angles $\alpha_i \sim 1.0°$.[24] A further description of the reflectometer setup is given in ref 25. Model fits to the data were calculated using a matrix formalism.[26] The interfaces are described by a tanh refractive index profile with the interfacial roughness $\sigma$. This profile is commonly used for silicon substrates[27] as well as for the interface between polymers.[16] In the case of polymer interfaces it is based on the volume fraction profile $\phi$ of one component, which can be described by a tanh profile to a good approximation.[28] Deviations originating from a concentration dependence of $\chi$ or the limited validity of the used approximations in the calculation of $\phi$[29] are neglected. The interface profile of the dewetted layer was parametrized in accordance with the results of the analysis of the atomic-force microscopy and optical phase interference microscopy data and not varied in the fit. A comparable method to analyze X-ray reflectivity curves of non-Gaussian surfaces using the information of AFM measurements is reported by Vignaud et al.[30] One has to consider that in the X-ray reflectivity measurements the density profile laterally averaged over the sample is determined. Therefore, holes in the film cause a reduction of the apparent scattering density of the material.

**Atomic-Force Microscopy.** Micrographs of the blend film were recorded with a Burleigh ARIS-3300 Personal atomic-force microscope (AFM). A standard Burleigh AFM probe was used for the measurements. The cantilever, with a silicon pyramidal tip, had a spring constant of $\cong 0.05$ N m$^{-1}$. The image acquisition in the constant-force (typically 8.4 nN) imaging mode was done in air at room temperature. Several images were obtained for each sample. The scan range was 5 $\mu$m × 5 $\mu$m to achieve a high resolution compared to the optical methods applied. The background due to the scanner tube movement is not fully subtracted from the data, which gives rise to the appearance of a long waviness if the surfaces are smooth. Therefore, the values of the root mean square (rms) roughness were only measured over an area of 1 $\mu$m × 1 $\mu$m. Additionally, some measurements were performed with a PARK Autoprobe AFM in noncontact mode to minimize tip-induced sample degradation. They exhibited the same topographic features.

**Optical Phase Measurement Interference Microscope.** For an optical characterization of the samples with a lateral resolution of approximately 1 $\mu$m and a height resolution better than 10 Å, a LOT/ZYGO phase measurement interference microscope was used. The interference pattern of monochromatic light reflected from a flat reference surface and the investigated sample is recorded in an area detector while the reference plane is moved with a piezoelectric device.[31] A magnification of 100 times was used. The area from which a data analysis is performed is 42.2 $\mu$m × 42.2 $\mu$m.

**Static Secondary Ion Mass Spectroscopy.** Static secondary ion mass spectroscopy (Static SIMS) analyses were performed using a Vacuum Science Workshop ion gun, operating with a 3 keV argon ion beam at a current of $2 \times 10^{-10}$ A measured at the gun exit, irradiating an area of $\cong 5$ mm$^2$. The geometry of the SIMS instrument is the incident beam at 45° to the sample and the secondary ions are detected normal to the sample surface. Due to the small features shadowing effects are negligible. Spectra were obtained with a Vacuum Generators 12-12 quadrupole, fitted with an Einzel lens energy filter. Sample charge compensation was achieved and necessary, with a flood gun providing 30 eV electrons.

## Results

**X-ray Reflectivity.** The bare, cleaned substrate and the polymer blend samples before annealing and after each annealing step were examined using X-ray reflectivity. The data together with a fit using the model explained in the Experimental Section are displayed in Figure 1. The data of the bare substrate (dry) show the typical $q_z^{-4}$ decay. From the fit we determine a surface roughness of 3 ± 1 Å. The reflectivity curve of the polymer blend film right after preparation (without) is dominated by well-pronounced fringes that originate from a homogeneous layer with a film thickness of 504 ± 9 Å. The determined surface roughness from the fit is 10 ± 2 Å. Regarding the first five annealing steps (30 min to 48 h), the fringes were damped out at higher $q_z$ values that correspond to an increase of surface roughness up to 26 ± 2 Å. Although in the reflectivity curves that correspond to the next two annealing steps (64 and 79 h) a few fringes are still left, we need to split the density profile into two layers of different electron densities. The layer near the substrate has a density value of bulk dPS and the upper layer a value of bulk PpMS. This indicates the formation of a bilayer system. Additionally, the surface roughness is further increased to 33 ± 3 Å. After annealing for 95 h, the surface roughness has increased to 64 ± 5 Å, and we detect no more fringes in our reflectivity data. During further annealing (191 h up to 911 h), fringes in the data reappear. Their $q_z$ spacing is doubled compared to the ones of early annealing times and with increasing annealing time they get more pronounced. This may be interpreted as a homogeneous layer of dPS near the substrate and a dewetted layer of PpMS on top. With increasing annealing time we observe the dewetting of the top layer to form micrometer size drops. With

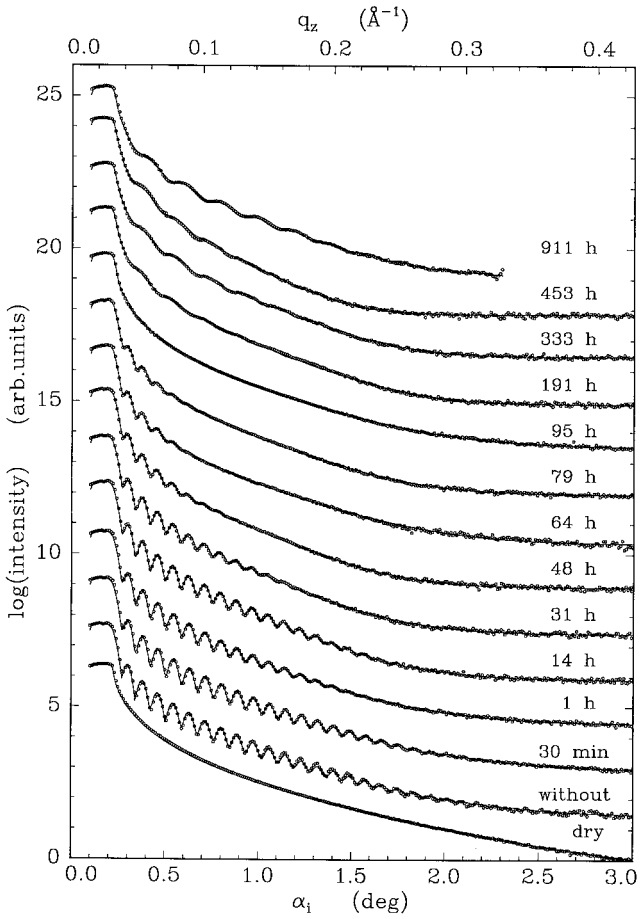


**Figure 1.** Specular reflectivity's (dots) and fits (solid lines) versus $q_z$ ($\lambda$ = 1.54 Å) of thin dPS/PpMS blend films on Si substrates at 12 different annealing times. For clarity the curves are shifted by 1 order of magnitude against each other. The cleaned substrate (dry) and the blend film as prepared (without) are presented for a comparison.

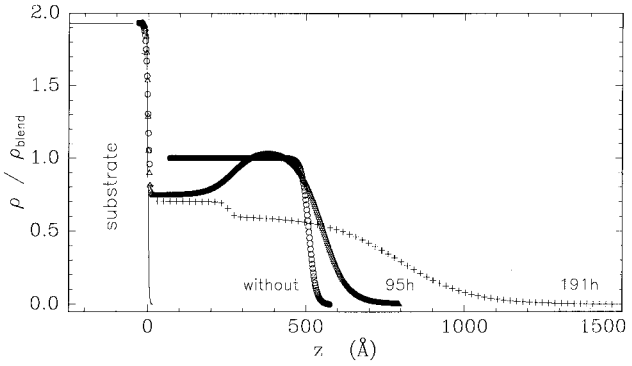


**Figure 2.** Example of three different density profiles of the dPS−PpMS blend thin film. The Si substrate is marked by the solid line. The density is normalized to the mean value of the symmetric bulk blend dPS−PpMS. The density profile of the sample right after preparation (circles) exhibits a uniform density corresponding to this mean value. After 95 h annealing time (triangles), two layers of different density, the bilayer system, are established. Note that, due to the big roughness values of the polymer−polymer interface as well as of the polymer−air interface, the density of the dPS layer seems to be increased and the density of the PpMS layer correspondly decreased. The density profile of the dewetted sample after 453 h annealing time (crosses) pictures the big roughness due to large drops.

increasing drop size, their contribution to the interface roughness extends until no fringes are observed in our experiment while the contribution of the smooth dPS−air interface in the coherently illuminated area increases. Both effects together lead to the observed reappearance of fringes. Figure 2 displays three typical density profiles, (i) of the homogeneous blend film, (ii) of the bilayer configuration, and (iii) of the dewetted sample, as obtained from the fit to the reflectivity data. The density value of the homogeneous layer is equal to the mean value calculated from the symmetric polymer composition. The surface roughness of the dewetted PpMS film cannot be measured with X-rays. Therefore the density profile has to be modeled from the bearing analysis of the AFM and PMIM measurements under the boundary condition of mass conservation.[30]

**Atomic-Force Microscopy.** The topography of the sample surface is measured with AFM at high resolution. Figure 3 displays six typical pictures as obtained at different annealing times. Right after preparation (Figure 3a) the surface is dominated by small dimples with a mean diameter of 3000 Å, which give rise to the observed surface roughness in the X-ray reflectivity data. From the low contrast of Figure 3a it can be concluded that the dimples have no sharp definition. The determined value for the surface roughness of 13 ± 2 Å is in good agreement with the rms value of the X-ray experiment. While with the AFM the roughness was measured over an area of 1 $\mu$m$^2$ with X-rays, a significantly larger area is examined. Consequently, the as-prepared samples have no dominant further long-wavelength roughness contributions. This very regular surface topography built up during the spin-coating and was previously similarly observed in the case of other polymer blend systems, too.[17,32,33] Annealing leads to changes in the surface topography (Figure 3b,c). The observed structures are less regular, and the peak to valley distances are increased. They can be assumed to arise from the progress of the phase separation process. After 90 h annealing time (Figure 3d), the in-plane structures increase significantly and the formed structures are still irregular. Due to the large structure size compared to the analyzed area, the resulting values of the rms roughness given in Table 1 are not representative of larger surface areas. This leads to deviations from data obtained by X-ray reflectivity or PMIM. With increasing annealing time, the drop diameter increases further and the contact line of the drops with the underlying layer becomes more regular and pronounced. Due to the small scan range of 5 $\mu$m × 5 $\mu$m in the later stages of the annealing, the evolving dewetting structures are no longer resolvable. The drop diameter as well as the distance between the drops are bigger than the scan range. Consequently, in Figure 3f the surface appears smooth again, which is in good agreement with the X-ray results.

**Optical Phase Measurement Interference Microscope.** For a more detailed analysis of the late stages we use the PMIM. Due to the magnification of 100 times, the surface topography is measured with a decreased resolution but with an increased scan range as compared to the AFM measurements. The white square in Figure 4a−e marks an area of 42.2 $\mu$m × 42.2 $\mu$m, which represents the area from which the data analysis (rms values) was performed. Therefore, in each picture many drops of the dewetting structure are detected. Note that the black and white contrast represents relative heights and thus drops appear in white (Figure 4c−e) and the underlying film in black.

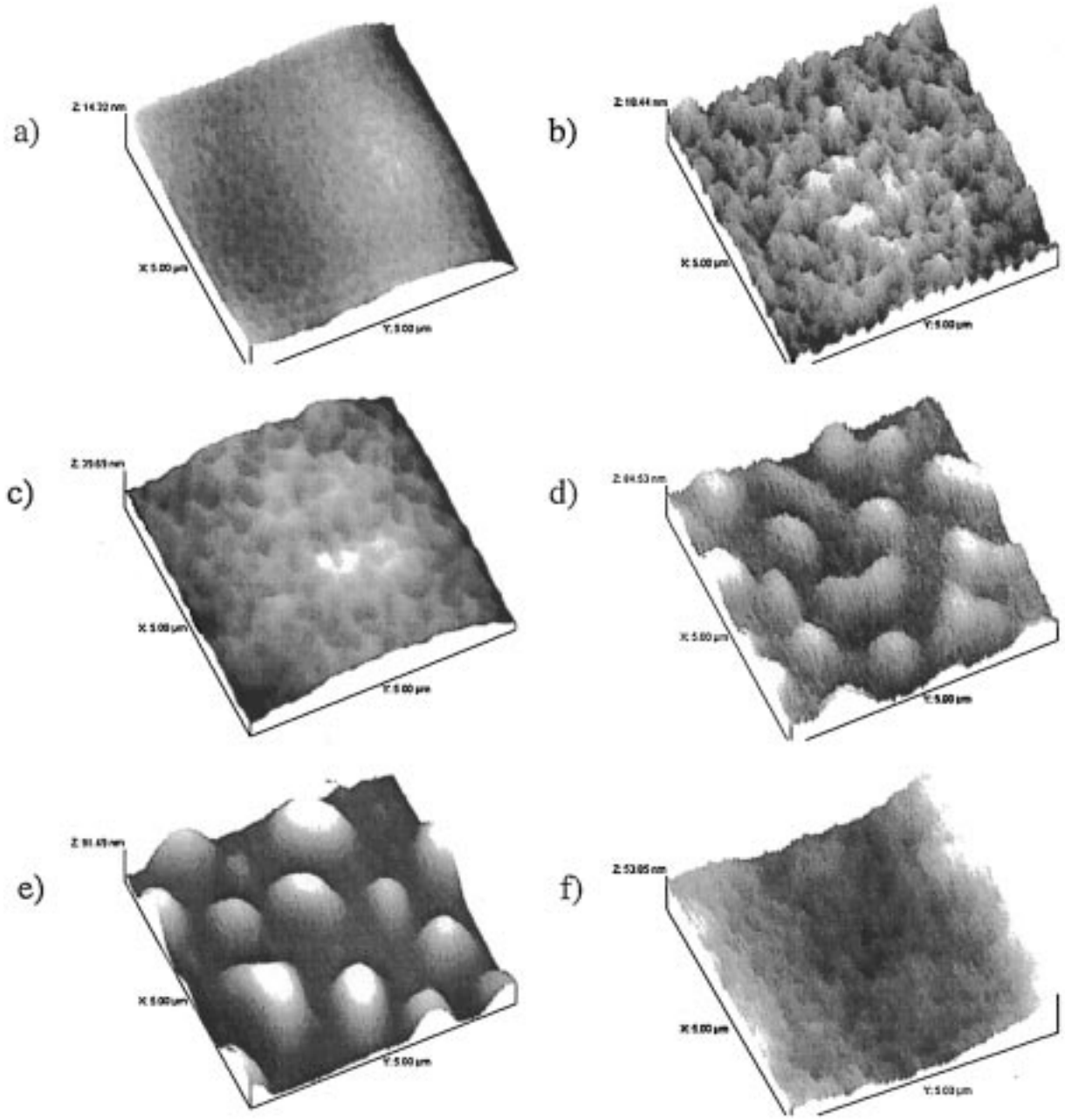


**Figure 3.** AFM images of the dPS−PpMS blend thin film at six different annealing times: right after preparation (a), 14 h (b), 79 h (c), 90 h (d), 95 h (e), and 454 h (f). The scan range of each picture is 5 $\mu$m × 5 $\mu$m whereas the *z* scale is different for each ((a) 14.32 nm, (b) 18.44 nm, (c) 39.69 nm, (d) 84.53 nm, (e) 91.49 nm, and (f) 53.85 nm) to show the in-plane structure more clearly.

After 79 h annealing time (Figure 4a), the surface shows a small surface roughness with a rms-roughness value of 35 ± 4 Å, which is in good agreement with the X-ray data. Figure 4b shows a stronger contrast due to the increased surface roughness (rms value 69 ± 5 Å) after 95 h annealing time. Figure 4c−e shows the development of the drop structure. The irregular-shaped drops (333 h, Figure 3c) as well as the elliptic-shaped drops (911 h, Figure 3e) have mean diameters of several micrometers. A numerical Fourier transform analysis of Figure 4b is presented in Figure 4f. It shows a ring that is typical for a spinodal process. The mean radius of this ring is $q_m = 0.36 \pm 0.08\ \mu m^{-1}$.

**Static Secondary Ion Mass Spectroscopy.** To obtain the surface composition of the samples, static SIMS measurements were performed, too. The spectra for the dPS and PpMS are in agreement with published data[34] and showed no significant impurities. The principal ion detected is at 98 Da for dPS, corresponding to the rearrangement of the aromatic ring and adjacent backbone methyne group to the relatively stable tropyllium ion, $C_7D_7^+$.[35] The PpMS homopolymer spectrum shows a principal ion at 105 Da, $C_8H_9^+$. The ion at 105 Da corresponds to the aromatic ring and the adjacent methyne forming a seven-membered ring, as with deuterated polystyrene, but also retaining the methyl substituent.[36] **All** blends showed a domination of PpMS at the surface since no dPS signal, i.e., 98 Da peak on SIMS spectra, was detected before and after annealing. It should be mentioned that static SIMS under the conditions used is sensitive only to the upper most atomic layer of the investigated samples. Thus it gives the chemical composition of the surface.

**Table 1. Variation of Surface Roughness and Topography as a Function of Annealing Time As Observed with X-rays, $\sigma_{X-ray}$, AFM, $\sigma_{AFM}$, and PMIM, $\sigma_{PMIM}$[a]**

| annealing time (h) | $\sigma_{X-ray}$ (Å) | topography | $d$ (nm) | $\sigma_{AFM}$ (Å) | $\sigma_{PMIM}$ (Å) |
|---|---|---|---|---|---|
| 0 | 10 | small holes | 207 | 13 | |
| 0.5 | 10 | | | | |
| 1 | 13 | granular | | | 14 |
| 14 | 13 | granular | 407 | 33 | |
| 31 | 18 | | | | |
| 48 | 26 | granular | | | 28 |
| 64 | 31 | | | | |
| 79 | 33 | granular | 351 | 49 | 35 |
| 90 | | drops | 1070 | (390) | |
| 95 | 64 | drops | 1333 | (510) | 69 |
| 191 | | drops | | | 157 |
| 333 | | drops | | | 187 |
| 453 | | drops | 3222 | (45) | 249 |
| 911 | | drops | | | 352 |

[a] Note the different in-plane length scales used in the analysis as mentioned in the text. Additionally, the mean in-plane dimension $d$ of the most prominent surface morphology is given.

## Discussion

**Model for dPS−PpMS Thin Blend Film.** While X-ray reflectivity delivers information perpendicular to the surface,[26,37−39] the in-plane structure of the samples is examined with AFM and PMIM. The size of the evolving structures varies over several orders of magnitude. From the static SIMS we get the chemical composition of the sample surface. The main results of all of the applied techniques are listed in Table 1. Note that the used techniques determine the surface roughness averaged over different in-plane length scales (X-ray 100 $\mu$m, PMIM 42.2 $\mu$m, and AFM 1 $\mu$m). Deviations between some of the determined surface roughness values thus arise from the different size of the sample areas probed with the different techniques. Consequently, the values of the AFM measurements have the biggest deviations due to the small examined range. In general, within the range of the experimental error the comparable values are in good agreement. Figure 5 shows the values of the surface roughness as determined by X-ray reflectivity and PMIM as a function of the applied annealing time. While during the phase separation process the surface roughness stays small, it increases significantly due to the drop formation, during the dewetting process. Although only examining a much smaller in-plane area this is significant from the AFM data, too. They show that the structure changes from a profile with features on the 1 nm scale to one with features on a 3−5 nm scale and then abruptly changes over 1 order of magnitude in scale as dewetting occurs.

Combining the results of all techniques, we can build a model for the thin blend film system dPS−PpMS. Right after the preparation by spin-coating up to annealing times of 911 h the topmost surface of the sample is dominated by PpMS, which results from the smaller surface tension $\gamma_{PpMS} = 35$ mN m$^{-2}$ compared to dPS $\gamma_{dPS} = 40$ mN m$^{-2}$ (values refer to room temperature[22]). dPS entraps PpMS during the rapid evaporation of the solvent, and this entrapped PpMS segregates to the surface of the dPS. Consequently, even in the late stages of the dewetting, a thin PpMS layer covers the homogeneous dPS layer. With X-ray reflectivity this thin top layer was not resolved, which indicates that its thickness is below the resolvable thickness of ≅15 Å given by the measured $q_z$ range.[40] A very thin layer of PpMS is also difficult to resolve because of the relatively small contrast to the dPS, in particular if the interface to the film below is relatively broad. Thus the sample as prepared appears as a homogeneous blend film with a mean density given by the symmetric composition of the blend. The measured surface roughness is due to small dimples at the surface. Since the overall free energy of immiscible films is lowered by minimizing the interfacial area between adjacent domains, the phase separation process will always tend to decrease the number of domains. This causes an increase of domain size, and thus an equilibrium stage of a phase separation process will never consist of more than two or three layers. The actual number is dependent on the polymer−interface interactions.[9] In the weakly immiscible system dPS−PpMS the phase separation leads to a bilayer system in which the once homogeneous film splits in two layers. The layer near the substrate is enriched with dPS, and the one near the surface consists of PpMS. The measured electron densities of each layer agree well with the bulk densities of the homopolymers, and the thickness ratio of dPS:PpMS = 250 Å:255 Å is consistent with the data for the symmetric composition. After 79 h of annealing time, we have a well-defined bilayer system with a broad interfacial width between the layers, which is caused by the weak incompatibility.[21,22] The measured value of $\sigma_{dPS-PpMS} = 65 \pm 8$ Å is equal to the value resulting from an annealing study of double-layer films.[23] These double-layer films were prepared with floating techniques and annealed for 19 h at 153 °C. With neutron reflectivity, an equilibrium bilayer interfacial width of $\sigma_{dPS-PpMS} = 67$ Å was determined.[22] Of course, starting with a blend system, a longer annealing time is necessary compared to investigations with a floated double-layer system. Note that the annealing time of 19 h in the work of Schnell[22] is necessary to reach equilibrium conditions for the bilayer system, which is not the equilibrium of the whole sample system, as the further dewetting process indicates. Thus, dewetting occurs in the bilayer samples, too.

This dewetting can be explained in terms of minimizing the surface free energy of the system. From the ratio of the surface tensions $\gamma_{PpMS}/\gamma_{dPS} = 0.875$ we can deduce a ratio of the Hamaker constants $A_{PpMSPpMS}/A_{dPSdPS}$ following the approximation of Frenkel $A \sim \gamma$.[41] A material with a smaller Hamaker constant is not stable on top of a material with a bigger one, which explains the dewetting of the upper PpMS layer. Due to the thickness of the underlying dPS layer the interaction with the silicon substrate is screened. Thus the calculation of the effective Hamaker constant, which determines the global wetting/dewetting behavior, cannot be performed as in a simple two-component system. Taking the literature values[42] of $A_{Si} = 22.5 \times 10^{-20}$ J and $A_{dPS} = 10 \times 10^{-20}$ J and the determined film thicknesses $l_{dPS} = 250$ Å and $l_{PpMS} = 255$ Å and following the approximation in ref 43, we calculate an effective Hamaker constant

$$A_{eff}(l_{PpMS}) = A_{PpMSPpMS} - A_{dPSPpMS} + \frac{A_{dPSPpMS} - A_{SiPpMS}}{(1 + d_{dPS}/l_{PpMS})^3} \quad (1)$$

Due to $A_{PpMSPpMS} < A_{dPSdPS}$ being independent of the thickness of $l_{PpMS}$, the effective Hamaker constant is

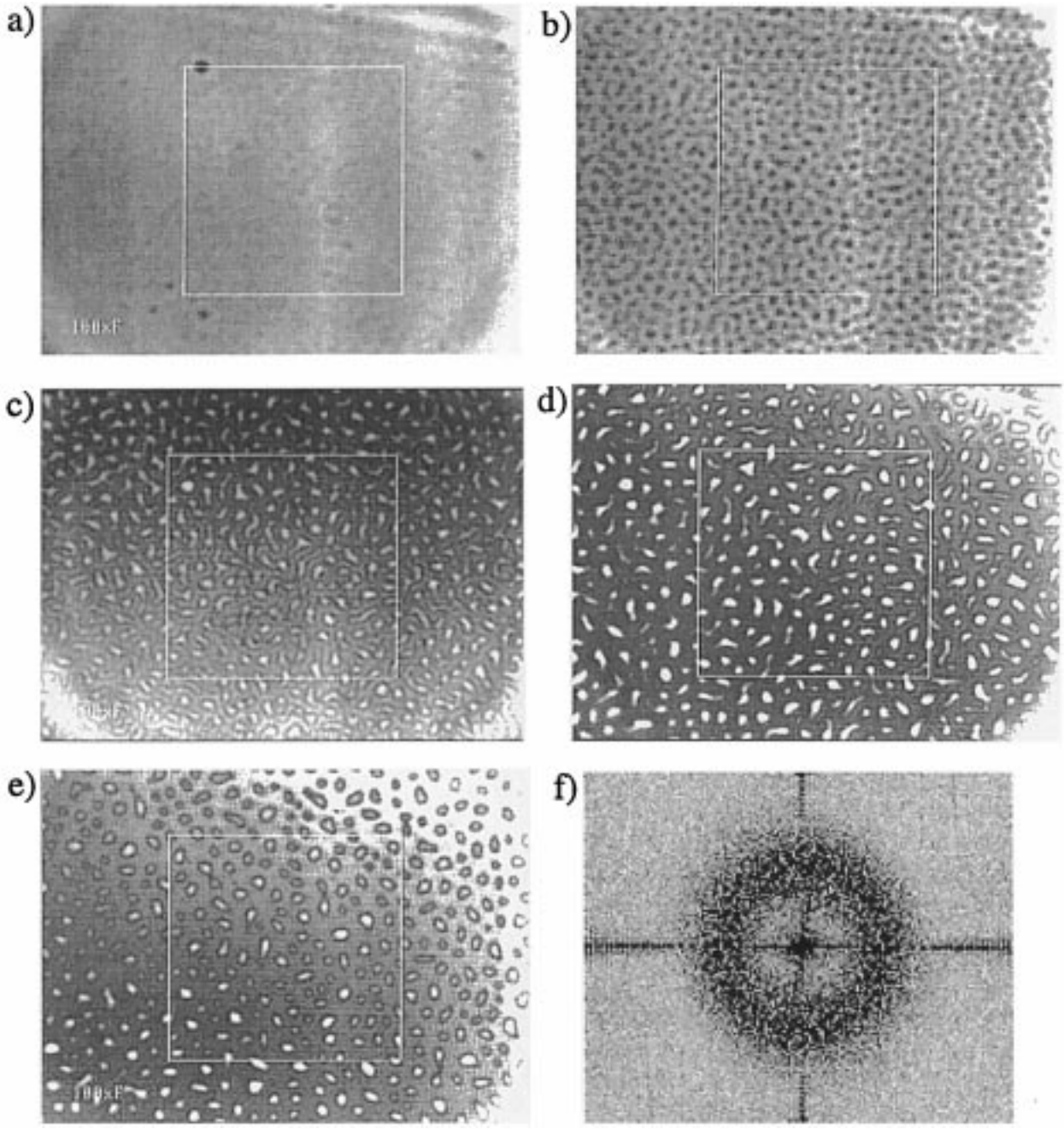


**Figure 4.** PMIM images of the dPS−PpMS blend thin film at five different annealing times: 79 h (a), 95 h (b), 333 h (c), 453 h (d), and 911 h (e). The white square marks an area of 42.2 $\mu$m × 42.2 $\mu$m. A numerical FFT of (b) is shown in (f). The $q$-axis are marked by solid lines.

always negative. Therefore, we conclude that no homogeneous film of PpMS can be stable on top of dPS. For the measured film thickness $l_{\mathrm{PpMS}} = 255$ Å we calculate $A_{\mathrm{eff}} = -1.19 \times 10^{-20}$ J. Therefore, the bilayer system is also unstable. The PpMS layer dewets on top of the dPS layer, while the dPS layer remains stable up to 911 h of annealing. After 95 h annealing time, the surface topography shows a regular structure that gives rise to a ring in the numerical FFT with a value $q_{\mathrm{m}} = 0.36 \pm 0.08\ \mu\mathrm{m}^{-1}$. From the spinodal model proposed for the dewetting of a thin homopolymer film,[44] we get a fastest growing wave vector $q_{\mathrm{m}} = 2\pi\sqrt{3/2}a/{l_{\mathrm{PpMS}}}^2$ with $a^2 = -A_{\mathrm{eff}}/(6\pi\gamma_{\mathrm{PpMS}})$. The calculated value $q_{\mathrm{m}} = 0.4 \pm 0.1\mu\mathrm{m}^{-1}$ fits well with the determined one. The given error bar results from the big range over which Hamaker constants are listed in the literature.[42,45] Additionally the mean drop radius of the final drop structure resulting from the dewetting process is given by $r^2 = 2\pi/\Theta_{\mathrm{E}}\sqrt{-4\pi\gamma_{\mathrm{PpMS}}/A_{\mathrm{eff}}}l^3$, and the estimated value $r = 3\ \mu$m corresponds in the range of error to the mean radius of PpMS drops formed on top of a dPS layer. Dewetting of a PpMS layer on top of dPS was also observed in bilayer samples created with floating techniques.[22] Because in systems built up by the floating technique, small cavities, some amount of water, dust particles, and folds at the interface cannot be avoided, the time scale on which dewetting sets in was strongly sample dependent and no reproducible value was determinable. Additionally, the resulting structures exhibited no spinodal ring when numerically transformed with FFT. Thus we conclude that in double-layer films prepared by floating techniques is the

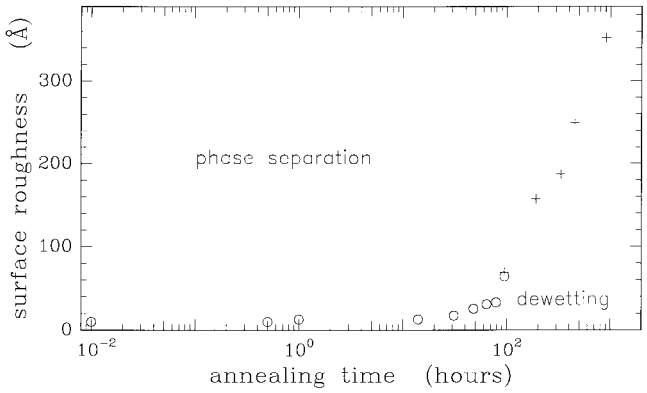


**Figure 5.** Resulting surface roughness from X-ray reflectivity (open circles) and PMIM (crosses) as a function of the annealing time of the dPS−PpMS blend thin film.

dewetting process driven by nucleation and growth and dependent on the amount of impurities at the interface between PpMS and dPS.

## Summary

Thin polymer films are well suited for the examination of dewetting because, due to the low vapor pressure and the high viscosity, the dynamic behavior is in an accessible time range. Investigating the dewetting of one polymer layer on top of another overcomes difficulties that arise from the substrate surface cleaning treatment. We note the possibility of creating bilayer systems from polymer blend films via phase separation. In contrast to the frequently used floating of one polymer layer on top of the other, with this technique we can avoid impurities such as folds or chemical heterogeneities at the polymer−polymer interface, which may act as grains for the dewetting process. Consequently in the presented study we detect a spinodal ring in the numerical FFT of a dewetting state. Although possible sample systems are limited to ones that are only weakly incompatible, there may be significant implications on the examination of polymer−polymer dewetting. In strongly incompatible systems the morphology originated during the spin-coating process can dominate the further dewetting.[46]

**Acknowledgment.** This work was partially supported by the European Community within program HCM-ERBCHBICT941717 and C11-CT-93-0351 as well as by a grant from DFG and a grant from EPSRC.

## References and Notes

(1) Gunton, J. D.; San Miguel, M.; Sahini, P. S. In *Phase Transitions and Critical Phenomena*; Domb, C., Lebowitz, J. L., Eds.; Academic: New York, 1983; Vol. 8.
(2) Redon, C.; Brochard-Wyart, F.; Rondelez, F. *Phys. Rev. Lett.* **1991**, *66*, 715.
(3) Reiter, G. *Phys. Rev. Lett.* **1992**, *68*, 75.
(4) Reiter, G. *Langmuir* **1993**, *9*, 1344.
(5) Redon, C.; Brzoska, J. B.; Brochard-Wyart, F. *Macromolecules* **1994**, *27*, 468.
(6) Martin, P.; Buguin, A.; Brochard-Wyart, F. *Europhys. Lett.* **1994**, *28*, 421.
(7) Lambooy, P.; Phelan, K. C.; Haugg, O.; Krausch, G. *Phys. Rev. Lett.* **1996**, *76*, 1110.
(8) Pan, Q.; Winey, K. I.; Hu, H. H.; Composto, R. J. *Langmuir* **1997**, *13*, 1758.
(9) Krausch, G. *Mater. Sci. Eng.* **1995**, *R14*, 1.
(10) Israelachvili, J. N. in *Intermolecular and surface forces*, 2nd ed.; Academic Press: London, 1991.
(11) Jones, R. A. L.; Norton, L. J.; Kramer, E. J.; Bates, F. S.; Wiltzius, P. *Phys. Rev. Lett.* **1991**, *66*, 1326.
(12) Bruder, F.; Brenn, R. *Phys. Rev. Lett.* **1992**, *69*, 624.
(13) Steiner, U.; Klein, J.; Fetters, L. *Phys. Rev. Lett.* **1994**, *72*, 1498.
(14) Krausch, G. *Ber. Bunsen-Ges. Phys. Chem.* **1994**, *98*, 446.
(15) Sung, L.; Karim, A.; Douglas, J. F.; Han, C. C. *Phys. Rev. Lett.* **1996**, *76*, 4368.
(16) Stamm, M.; Schubert, D. W. *Annu. Rev. Mater. Sci.* **1995**, *25*, 325.
(17) Affrossman, S.; Henn, G.; O'Neill, S. A.; Pethrick, R. A.; Stamm, M. *Macromolecules* **1996**, *29*, 5010.
(18) Dalnoki-Veress, K.; Forrest, J. A.; Stevens, J. R.; Dutcher, J. R. *Physica A* **1997**, *239*, 87.
(19) Tanaka, K.; Takahara, A.; Kajiyama, T. *Macromolecules* **1996**, *29*, 3232.
(20) Walheim, S.; Böltau, M.; Mlynek, J.; Krausch, G.; Steiner, U. *Macromolecules* **1997**, *30*, 4995.
(21) Jung, W. G.; Fischer, E. W. *Makromol. Chem., Macromol. Symp.* **1988**, *16*, 281.
(22) Schnell, R. Ph.D. Thesis, University of Mainz, 1997.
(23) Schnell, R.; Stamm, M. *Physica B* **1997**, *234−236*, 247.
(24) Tolan, M.; Bahr, D.; Süenbach, J.; Press: W.; Brinkop, F.; Kotthaus, J. P. *Physica B* **1994**, *198*, 55.
(25) Foster, M.; Stamm, M.; Reiter, G.; Hüttenbach, S. *Vacuum* **1990**, *41*, 1441.
(26) Lekner, J. In *Theory of Reflection*; Martinus Nijhoff Publishers: Dodrecht, 1987.
(27) Bahr, D.; Press: W.; Jebasinski, R.; Mantl, S. *Phys. Rev. B* **1993**, *47*, 4385.
(28) Binder, K. *J. Chem. Phys.* **1983**, *79*, 6387.
(29) Binder, K.; Frisch, H. *Macromolecules* **1984**, *17*, 2928.
(30) Vignaud, G.; Gibaud, A.; Paris, F.; Ausserre, D.; Grübel, G. To be published in *Thin Solid Films*.
(31) Biegen, J. F.; Smythe, R. A. SPIE O/E LASE'88 Symposium, Los Angeles, CA, 1988.
(32) Jandt, K. D.; Heier, J.; Bates, F. S.; Kramer, E. J. *Langmuir* **1996**, *12*, 3716.
(33) Kumacheva, E.; Li, L.; Winnik, M. A.; Shinozaki, D. M.; Cheng, P. C. *Langmuir* **1997**, *13*, 2483.
(34) Jones, R. A.; Kramer, E. J. *Polymer* **1993**, *34*, 115.
(35) Affrossman, S.; Hartshorne, M.; Jerome, J.; Munro, H. S.; Pethrick, R. A.; Petijean, S.; Rei Vilar, M. *Macromolecules* **1993**, *26*, 5400.
(36) Affrossmann, S.; Hindryckx, F.; Pethrick, R. A.; Stamm, M. In *Polymer-Solid Interface*; Pireaux, J. J., Bertrand, P., Bredas, J. L., Eds.; Institute of Physics Publishers: Bristol, PA, 1992; p 337.
(37) Parrat, L. G. *Phys. Rev.* **1954**, *55*, 359.
(38) Born, M.; Wolf, E. In *Principles of Optics*, 2nd ed.; Pergamon Press: Oxford, U.K., 1964.
(39) James, R. W. In *The Optical Principles of the Diffraction of X-rays*; OxBow Press: Woodbridge, CT, 1962.
(40) Schalchli, A.; Benattar, J. J.; Licoppe, C. *Europhys. Lett.* **1994**, *26*, 271.
(41) Frenkel, J. *Kinetic theory of liquids*; Dover Publications Inc.: New York, 1955.
(42) Visser, J. *Adv. Colloid Interface Sci.* **1972**, *3*, 331.
(43) Cazabat, A. M. In *Les Houches, Session XLVIII, 1988-Liquides aux Interfaces/Liquids at Interfaces*; Charvolin, J.; Joanny, J. F.; Zinn-Justin, J., Eds.; Elsevier Science Publishers B.V.: Amsterdam, 1990; p 374.
(44) Brochard-Wyart, F.; Redon, C.; Sykes, C. *C. R. Acad. Sci. Ser. 2* **1992**, *19*, 314.
(45) Müller-Buschbaum, P.; Tolan, M.; Press: W. *Z. Phys. B* **1994**, *95*, 331.
(46) Müller-Buschbaum, P.; Stamm, M. to be published.

MA971802Q